Toward quantitative assessment of deformational plagiocephaly and brachycephaly at the point-of-care

Reza Seifabadi,[a,*] Fereshteh Aalamifar,[a] Seyed Hossein Hezaveh,[a] Can Kocabalkanli,[a] Kelly Wilburn,[a,b] and Marius George Linguraru[a]

[a]PediaMetrix, Inc., Rockville, Maryland, United States
[b]Dunwoody Pediatrics, Dunwoody, Georgia, United States

Abstract

Purpose: Develop and validate algorithms that can enable a novice user to quantitatively measure the head shape parameters associated with deformational plagiocephaly and brachycephaly (DPB) using 2D rendered images.

Approach: First, the head contour is extracted semi-automatically using the intelligent scissors method. We then automatically compute two indices used in the clinical determination of the DPB from the head shape parameters: the cranial index (CI) and the cranial vault asymmetry index (CVAI). We also present methods to quantify and compensate for the user variability, including camera angle and distance from the head using 2D rendered images. We compared the results of our technology with ground-truth (GT) measurements from 53 infants with DPB and normal cranial parameters.

Results: The Spearman correlation coefficient between the new 2D rendered method and the 3D GT was 0.94 ($p < 0.001$) and 0.96 ($p < 0.001$) for CI and CVAI, respectively. Different simulated camera angles and distances from the head resulted in variation in CI and CVAI in the range of $[-2.0, 6.0]$ and $[-4.0, 4.0]$ units, respectively. The limits of agreement of the Bland–Altman test were reduced from $[-3.6, 5.3]$ and $[-3.6, 4.2]$ to $[-0.5, 3.0]$ and $[-1.3, 1.6]$ for CI and CVAI, respectively, by combining results from different camera angles and positions in our method. The overall accuracy of the proposed technology for DPB detection was 100%.

Conclusions: The 2D rendered images of the head can be accurately analyzed to assess DPB. Further study on 2D photos taken from human subjects is warranted.

 [DOI: 10.1117/1.JMI.8.2.024504]

Keywords: head deformity; pediatrics; point of care; quantitative imaging; smartphone.

Paper 20263RR received Sep. 29, 2020; accepted for publication Apr. 13, 2021; published online Apr. 29, 2021.

1 Introduction

About 20% to 30% of newborns manifest moderate to severe head deformation in the first months after birth,[1] and delayed identification causes significant medical and societal costs. The most common infant head deformations are deformational plagiocephaly and brachycephaly (DPB) [see Fig. 1(a)]. These conditions require immediate attention and benefit from early treatment. Abnormal head shape or growth patterns in infants are correlated with other health conditions such as developmental delays, torticollis, microcephaly, and hydrocephalus.[1–11] In addition, these children and their families are affected by social stigma and psychological pressure.[12] Therefore, it is essential to monitor the growth of infant heads to be able to initiate early and less invasive therapy for children with head deformation, i.e., to prevent the need for helmet therapy for DPB, and associated health complications.[13–17]

The incidence of DPB has risen from 2%–5% to 20%–46% since the back-to-sleep campaign[1,18] to avoid sudden infant death syndrome, causing DPB to be called a pediatric

*Address all correspondence to Reza Seifabadi, reza.seifabadi@pediametrix.com

2329-4302/2021/$28.00 © 2021 SPIE

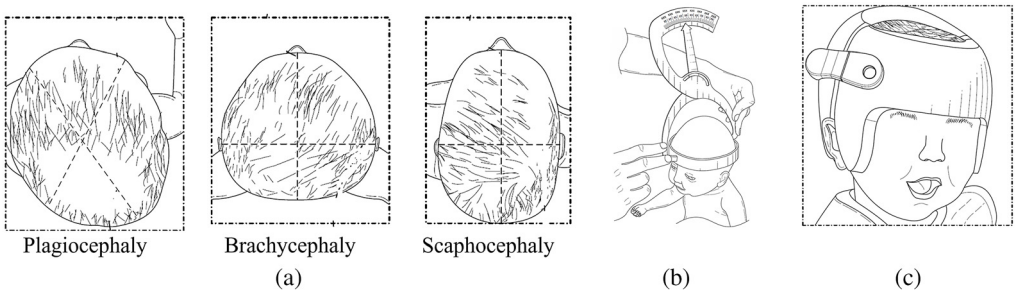

Fig. 1 Measurement and management of DPB. (a) Types of DPB: plagiocephaly when the head is asymmetric; brachycephaly, when the head is wider than normal; and scaphocephaly, when the head is longer than normal. (b) A craniometer to measure DPB by a specialist. (c) Correctional helmet for treatment of DPB.

epidemic.[19] For diagnosis, families are referred by a pediatrician to orthotists or pediatric neurosurgeons who use a mechanical caliper called craniometer[20] [Fig. 1(b)] or 3D imaging[21] to determine the type and severity of the cranial deformation. It can take up to two months to schedule such visits, leaving parents in anxiety and potentially missing the opportunity to correct DPB by conservative therapy,[18] which is effective only in the first 4 to 6 months of life.

A critical challenge in the early detection of cranial deformations is the absence of tools available to pediatricians to perform quantitative head shape assessment during brief well-child visits. Typically, only the head circumference of the infant is measured, using a tape. Moreover, head shape evaluation performed by specialists is done only for the indication of cranial deformation. As a result, over 600,000 infants remain untreated every year in the U.S. for their head deformations.[19] Thus, there is a critical need to develop and disseminate objective tools for simple, low cost, and reproducible assessment of cranial shape in pediatrician offices.

In this paper, we first present algorithms that enable the semi-automatic measurement of the head shape parameters associated with DPB from top-view 2D rendered images from 3D scans of the head. We also simulated the effect of user variability errors, such as the camera angle and distance from the head, and landmark selection (the tip of the nose) on the accuracy of the cranial shape parameters. Then, we propose methods to compensate for the user variability error. Finally, we report the accuracy of our technology using 2D rendered images of infants with DPB and normal cranial shape.

2 Materials and Methods

2.1 *Data*

We used retrospective, curated 3D data from 53 patients with DPB or normal head (33 with plagiocephaly/brachycephaly, 2 scaphocephaly, and 18 normal head shape). The dataset was acquired using 3dMDHead System (3dMD, Atlanta, Georgia) or STARscanner (Orthomerica, Orlando, Florida). All data were de-identified prior to the study.

2.2 *Measurement of Head Shape Parameters from 2D Photographs in the Absence of User Variability Error*

The type and severity of DPB are characterized from two cranial metrics: the cranial index (CI) and cranial vault asymmetry index (CVAI).[22] These indices are typically measured using calipers by clinical specialists, such as physical therapists, orthotists, or neurosurgeons. It was shown that a 2D top-view photo of an infant's head, which was manually analyzed by experts to calculate CI and CVAI, can be used to characterize DPB.[22] Nevertheless, the feasibility of systematically and accurately calculating these parameters remained to be verified. For these reasons, we developed methods and image processing algorithms to interactively extract the head contour from a top-view photo of the head and automatically calculate CI and CVAI.

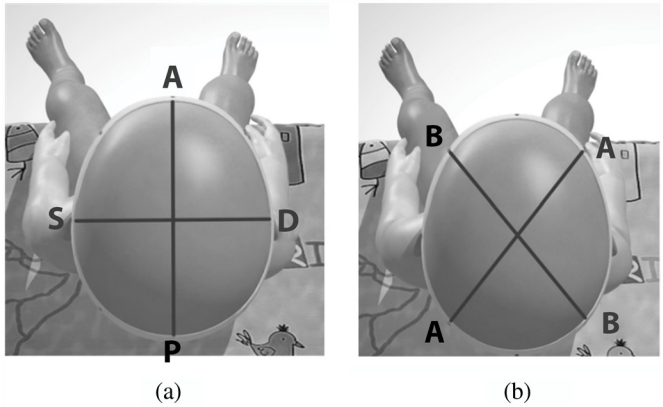

Fig. 2 (a) Calculation of CI $=$ SD $\times$ 100/AP and (b) calculation of CVAI $= \frac{AA-BB}{\max(AA,BB)} \times 100$ (40 deg from the nose direction).

Fig. 3 A flowchart showing the steps taken to calculate CI/CVAI.

Accurate extraction of the head contour is a prerequisite to measurement of CI and CVAI. In our initial approach, the user clicks 6 to 10 points that roughly trace the head contour on the picture. Then, the contour is refined using the intelligent scissors algorithm[23,24] in which a graph is constructed from the image using the seeds. Then the Dijkstra algorithm[25] is used to find the optimal path between consecutive seed points,[26] which is smoothed using a piecewise cubic spline.

Given the head contour, the CI and CVAI are calculated using a method similar to what was illustrated by Schaaf et al.[22] CI and CVAI are calculated as CI $=$ SD $\times$ 100/AP, CVAI $= \frac{AA-BB}{\max(AA,BB)} \times 100$ based on Schaaf et al.[22] (Fig. 2). In that study, however, human experts manually measured certain landmarks (including nose tip and ears) for the measurement of CI and CVAI. Similarly, we use the tip of the nose as one of the landmarks to define the nose direction. Instead of using ears as other landmarks (which may not appear in the image), we used center of the mass of the head contour to define the nose direction from which CI and CVAI are calculated. We use the shape indices to both determine if DPB is present and to differentiate between left and right conditions when relevant.

Figure 3 shows the steps taken to calculate CI/CVAI.

We compared the results of our algorithm on 2D rendered images with ground-truth (GT) measurements from 53 retrospective, 3D datasets with DPB and normal cases. The GT was obtained from 3D scans of the head using methods described by Sato et al.[27] Our measurements were performed on 2D rendered images of the head. The CI and CVAI ranged from 72 to 102 (mild scaphocephaly–severe brachycephaly) and 0 to 15 (normal–severe plagiocephaly), respectively. Analysis was performed by the Spearman correlation test and a linear regression model between the 2D and 3D measurements. The overall accuracy, sensitivity, and specificity of our method for the identification of DBP were also measured and reported.

2.3 *Quantify and Compensate for the Effect of User Variability on the Cranial Shape Measurements*

2.3.1 *Quantify for camera angle and distance*

The notion of apparent contour can best describe the effect of camera angle and distance on CI and CVAI measurements. Apparent contours are the projection of the contour generators, as shown in Fig. 4, for a given angle and distance from the target (i.e., the head), which separate the visible and occluded parts on a surface.[27] In other words, the apparent contour is what

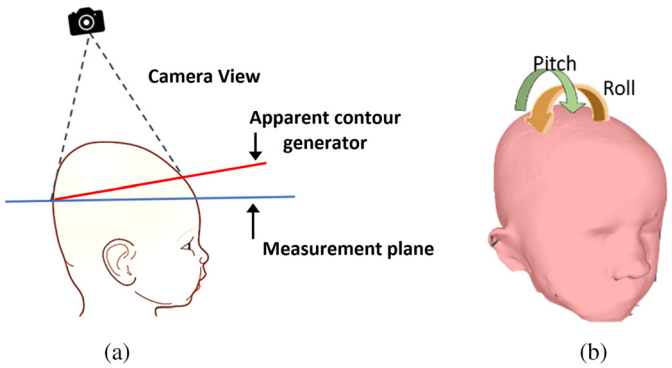

Fig. 4 Effect of camera input: (a) two different apparent contour generators can lead to two different top-view photos; (b) pitch and roll angles to generate apparent contours and simulate user input variability.

appears in the photo and is a function of the GT contour, as well as of the camera angle, camera-to-head distance, and camera parameters. The measurement plane is a plane that parallels to the XY plane at the level of the largest head circumference. The XY plane is defined based on certain anatomical landmarks (the left and right tragions, nasion, and subnasal). The virtual camera had a focal length of 31 mm to simulate an iPhone 6 camera.

To quantify the effect of extrinsic camera angle variation, we used 53 cranial surfaces from DPB and normal head shapes. Through simulations, we generated top-view 2D projections of the head to study the effect of the camera angle and distance on the accuracy of cranial shape parameters. As shown in Fig. 4(b), to generate apparent contours, two angles were defined for the relative pose of the camera to simulate the effect of variable input by novice users. Pitch and roll were varied from -6 deg to 14 deg and -8 deg to 8 deg, respectively (these large variations are exaggerated). The camera distance was set at 300, 400, and 500 mm from the head. In total, 507 2D projections were generated from every 3D volume.

Next, the head contour was automatically extracted from the simulated 2D pictures. To perform this automatic extraction, the nose and ears were removed using a separate image cropping method to isolate the head shape. CI and CVAI values were computed based on our methods described earlier. We then computed the CI and CVAI from top-view pictures selected by an expert user.

2.3.2 *Compensation for camera angle and distance*

To reduce the variability in measurement from different camera angles and positions, we used a few frames at random angles and averaged the results. We observed that the effect of novice user input can be substantially reduced using this method that analyzes multiple data points, thus increasing the accuracy of the computation of cranial shape parameters used for the clinical evaluation of DPB. We then compared CI and CVAI (computed from angles selected by an expert user) with those from "novice users" (one image selected at random angle and distance within the specified range defined above) and with "our method" (combination of 5 or 10 images selected at randomly distributed angles and distances).

2.3.3 *Quantify and compensate for the effect of nose direction*

As described earlier, measurements of CI and CVAI require the user to select the tip of the nose within the 2D picture. We minimized the variability in the selection of the nose direction using the centroid of the head contour (COM method). Yet, the manual selection of the nose tip can contribute to variations in CI and CVAI, thus affecting the classification and severity determination of DPB. In this section, we investigated the effect of nose selection on CI and CVAI.

Using the cranial surfaces described earlier, this study was performed in two phases:

1. Systematic study: find the sensitivity of CI/CVAI measurements to the nose-tip selection by systematic error analysis.

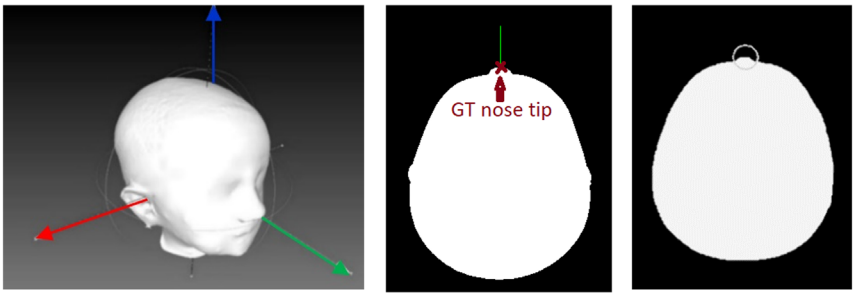

Fig. 5 Systematic error analysis for the nose-tip selection. (a) Head volume with green-axis marking the nose tip; (b) the top-view projection generated from the head volume shown in (a) at camera distance of 400 mm and no rotation of the camera angle (the GT nose tip is defined as the intersection of the green line and the head contour); and (c) the region of error equivalent to a radius of 20 pixels.

2. Intra-user and inter-user variability study: quantify the expected nose-tip selection error through a user study with five participants, each repeating nose-tip selection five times for all 2D images.

Systematic study. Top-view projections at perfect camera angle and three different camera distances (300, 400, and 500 mm) were generated from each of the 53 head volumes. An example head volume is shown in Fig. 5(a), and an example top-view projection is shown in Fig. 5(b). The green axis shown in Fig. 5(a) was defined to pass through the nose tip so that the GT nose-tip location can be extracted automatically by intersecting the green line and the head contour as shown in Fig. 5(b). Hence, 159 top-view photos with their GT nose tips were generated. For each photo, systematic errors with radius $R = 0{:}10{:}100$ pixels and angle $\theta = 0{:}45{:}135$ deg were generated at the nose-tip location.

3 Results

3.1 *Accuracy of 2D-Rendered Method Compared to 3D Measurement in the Absence of User Variability*

The Spearman correlation coefficients between our method and the GT 3D measurements were 0.949 ($p < 0.001$) and 0.964 ($p < 0.001$) for CI and CVAI, respectively. The regression analysis demonstrated an improvement of the error in the measurements from 2.2 ± 0.5 to 1.9 ± 0.3 for CI ($p < 0.05$) and from 1.5 ± 0.4 to 1.3 ± 0.3 for CVAI ($p < 0.001$). These results indicate that the regression can be effective (Fig. 6).

3.2 *Effect of User Variability on CI and CVAI*

Figures 7(a) and 7(b) show an example of the effect of the variability in camera angle and distance. The CI error range was $[-6,2]$ and the CVAI error range was $[-5,5]$. The CI typical range is [65, 105] and the CVAI typical range is $[-23,23]$. Although this large variation in simulated extrinsic camera parameters may be exaggerated, the wide range of errors can result in incorrect diagnosis and classification of severity of DPB.

In general, the effect of the camera distance from the head was more pronounced on CI than CVAI, whereas the effect of the roll angular error was more evident on CVAI than CI. The effect of roll angular error was observed to be symmetrical in most cases, i.e., a positive angular error created a positive shift in CVAI, whereas a negative angular error resulted in an opposite effect. The effect of the pitch angular error on CI was notable in the positive direction, i.e., leaning forward toward the face. To minimize the effect of camera angle, landmarks were used during data collection to limit the possible acceptable range of camera angle and distance.

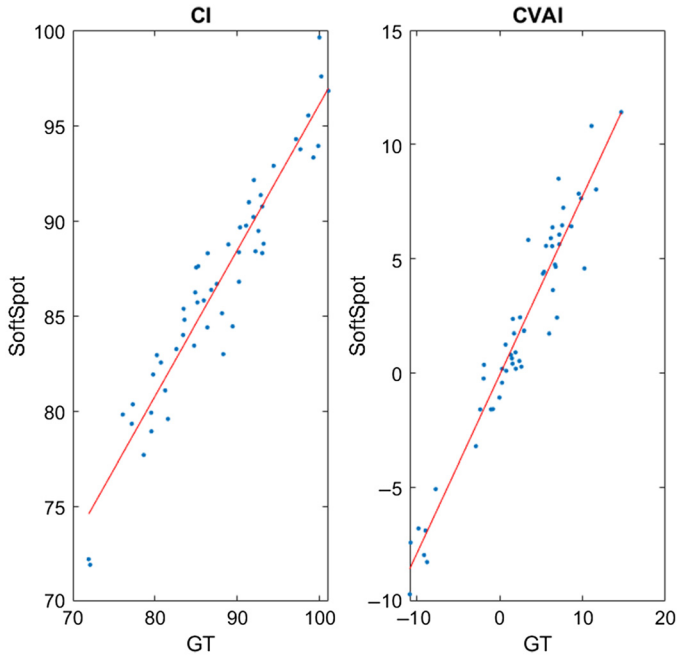

Fig. 6 Results of regression analysis comparing results from SoftSpot to those of GT using a least square linear regression (red line). The Spearman correlation coefficient between the new method and the GT was 0.949 ($p < 0.001$) and 0.964 ($p < 0.001$) for CI and CVAI, respectively.

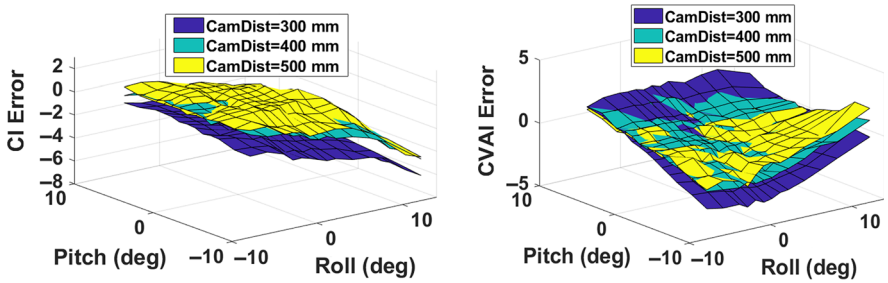

(a) (b)

Fig. 7 The effect of pitch and roll angles on (b) CI and (c) CVAI.

3.3 *Compensate for User Variability*

We systematically simulated the effect of user input on image acquisition and analysis on the computation of CI and CVAI. We proposed methods to compensate for these errors, which improved the limits of agreement (LoA) within 95% of confidence interval in the Bland–Altman plot analysis for CI and CVAI to $[-0.5, 3.0]$ and $[-1.3, 1.6]$ respectively. Table 1 and Fig. 8 show how our method compensates for the effect of user input by novice users. These findings demonstrate that our approach significantly reduces the error in the computation of cranial shape parameters. Table 1 also suggests that using more random angles (10 versus 5) does not noticeably increase the accuracy of our algorithms.

3.4 *Effect of User Variability on DPB Detection*

3.4.1 *Systematic error analysis*

Figure 9 shows how sensitivity and specificity of DPB detection change as the radius of the nose-tip error increases. We noted that the nose-tip selection error has higher impact on specificity

Table 1 Results of compensation for the effect of camera angle and distance demonstrated by the LoA in the Bland–Altman test.

	LoA in CI	LoA in CVAI
A random shot (novice user)	[−3.6, 5.3]	[−3.6, 4.2]
Our method (5 random angle)	[−0.9, 3.2]	[−1.4, 1.6]
Our method (10 random angles)	[−0.5, 3.0]	[−1.3, 1.6]

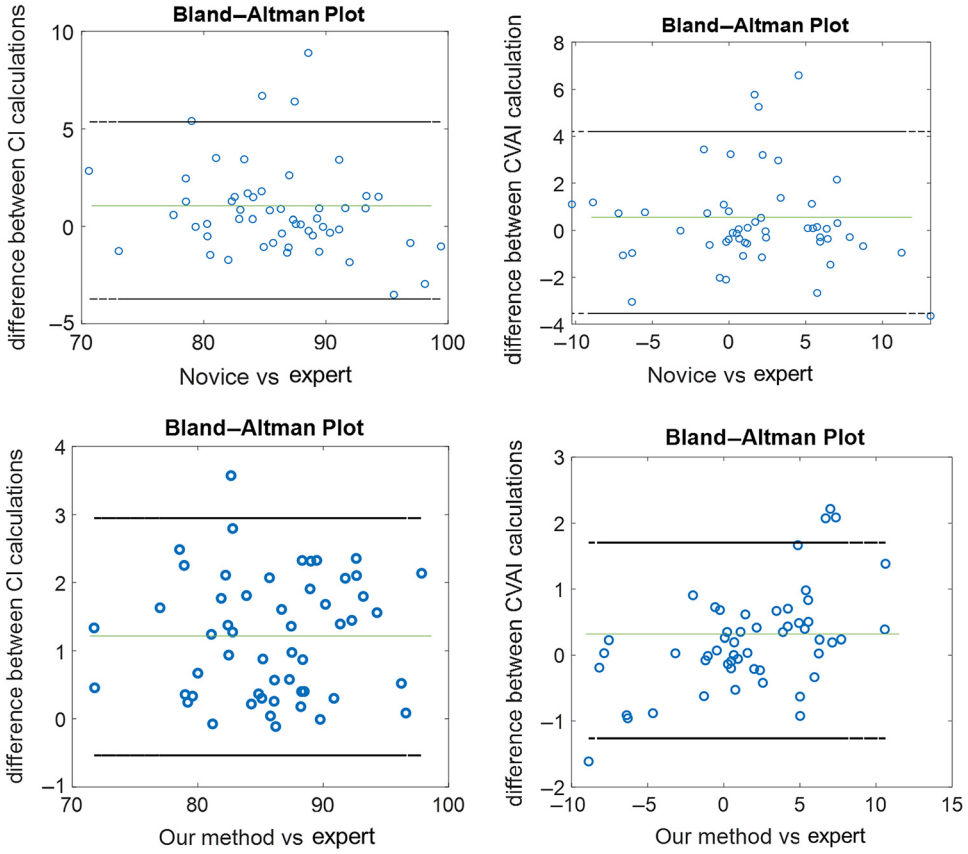

Fig. 8 Bland–Altman plot comparing our method and novice user versus expert. Black lines show LoA and green line shows the bias. Notable improvement in LoA can be seen with our method (bottom row).

than sensitivity. However, if the error stays within 10 pixels, 92% specificity and 99% sensitivity can be expected for the detection of DPB. Increasing the flexibility in the selection of the nose tip to 20 pixels degraded the specificity to 82% but still warranted a sensitivity of 98%.

3.4.2 *Intra-user and inter-user variability study*

We asked five users with varying familiarity with the project to select the nose tip. Each user repeated this experiment five times for each of the 159 top-view photos. Figure 10 shows the radial (Euclidean) error, compared to GT, for all the trials. To prevent outliers, we required novice users to select the nose tip five times and outliers were removed. Table 2 shows the intra-user and inter-user variability after removing the outliers. Note that the mean variability is under 4 pixels, which guarantees high sensitivity and specificity for DPB detection, as noted above.

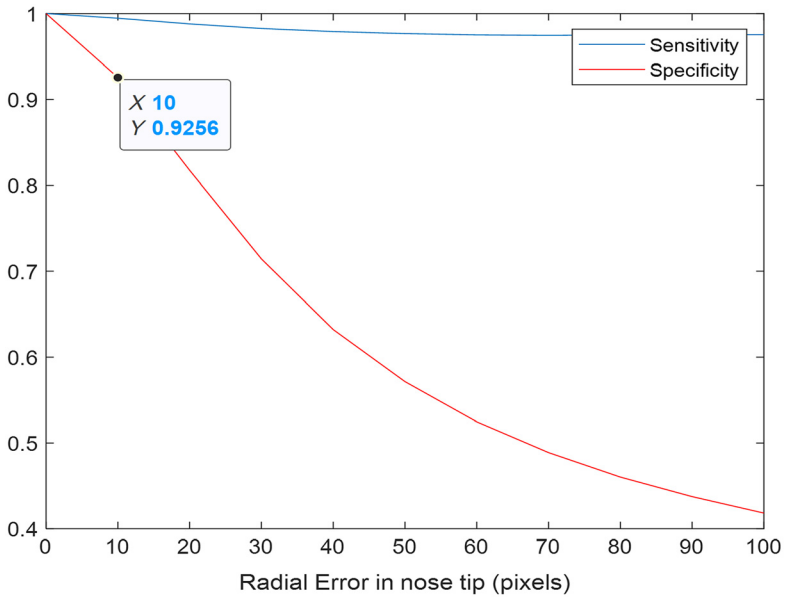

Fig. 9 Effect of the nose-tip selection. Sensitivity and specificity of DPB detection are plotted as a function of radial error in the nose-tip selection.

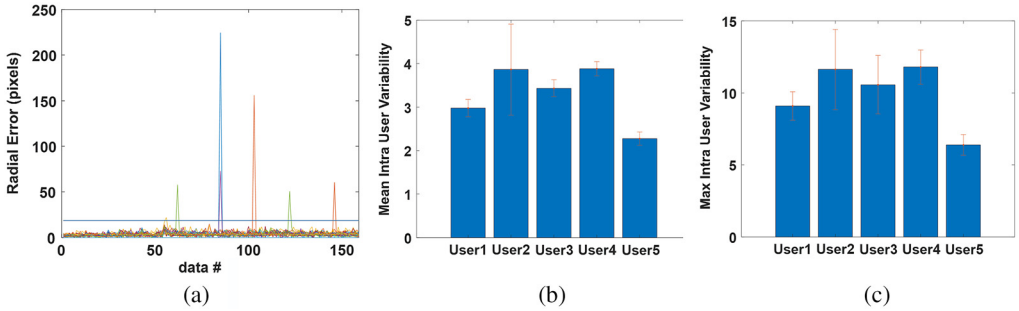

Fig. 10 Inter- and intra-user variability for the nose-tip selection. (a) Radial (Euclidean) error compared to the GT for all trials of all users. The solid line shows the mean + 3 * STD (= 18 pixels), where STD is the standard deviation. The mean radial error is 4 pixels. (b) Intra- and (c) intra-user variability for each user when they repeated the nose-tip selection five times.

Table 2 Inter-user and intra-user variability for the selection of the nose tip after removing the outliers.

	Mean (pixels)	Max (pixels)
Inter-user	3.8 ± 0.7	11.6 ± 2.2
Intra-user	3.3 ± 0.4	9.9 ± 0.8

3.5 *Overall Accuracy Study*

Using the 53 3D datasets of DPB and normal cases, we compared the GT with the DPB detection and classification results of our methods (SoftSpot) when the effects of the user variability were eliminated. As shown in Table 3, SoftSpot was able to distinguish all DPB cases from normal ones successfully (100% accuracy) using the combination of CI and CVAI. Table 4 shows the confusion matrix for the classification of types of DPB.

Table 3 Evaluation of SoftSpot DPB detection.

	CI	CVAI	Combined
Accuracy	96%	96%	100%
Sensitivity	100%	94%	100%
Specificity	85%	100%	100%

Table 4 Confusion matrix for the classification of type of DPB using SoftSpot.

		Brachycephaly	Schaphocephaly	Normal
CI	Brachycephaly	40	0	0
	Schaphocephaly	0	2	0
	Normal	2	0	9
		Right plagiocephaly	Left plagiocephaly	Normal
CVAI	Right plagiocephaly	22	0	2
	Left plagiocephaly	0	7	0
	Normal	0	0	22

3.6 *Semi-Automatic Segmentation*

Currently, our algorithms for segmentation and selection of the landmarks are semi-automatic as described in this paper. This means the analysis of the images collected via the mobile application was performed off-line on a computer by PediaMetrix's data analyst. These steps take less than 2 min per image. In future work, we will focus on the automation of our algorithms for real-time response.

4 Conclusions

We developed algorithms that can accurately assess the presence of DPB from top-view pictures of infant heads that can be acquired at the point-of-care. We quantified the effect of the user variability including camera angle, distance from the head, and selection of the nose tip on the measurement of cranial shape in a simulation study using 2D rendered images from 3D scans of the head. We also introduced methods that can compensate for user variability and significantly reduce the errors of these measurements. Our results with retrospective data showed 100% accuracy for the detection of DPB and proved the feasibility of our methods (SoftSpot) for the classification of types of DPB using 2D rendered images of the head scans.

Currently, our algorithms for segmentation and selection of the landmarks are semi-automatic, as described in Sec. 2. This means the analysis of the collected images via the mobile application is performed off-line by a data analyst. These steps take less than 2 min per image. In future work, we will focus on the automation of our algorithms for real-time response. Future studies will also be performed with larger and with human subject data.

Disclosures

Authors have financial interest in PediaMetrix, Inc.

Acknowledgments

This work was supported by the National Science Foundation SBIR Phase I, Award No. 1914051.

References

1. A. Mawji et al., "The incidence of positional plagiocephaly: a cohort study," *Pediatrics* **132**(2), 298–304 (2013).
2. I. Y. Moon et al., "Analysis of facial asymmetry in deformational plagiocephaly using three-dimensional computed tomographic review," *Arch. Craniofac. Surg.* **15**(3), 109–16 (2014).
3. B. R. Collett et al., "Development in toddlers with and without deformational plagiocephaly," *Arch. Pediatr. Adolesc. Med.* **165**(7), 653–658 (2011).
4. M. L. Speltz et al., "Case-control study of neurodevelopment in deformational plagiocephaly," *Pediatrics* **125**(3), e537–e54 (2010).
5. B. R. Collett et al., "Development at age 36 months in children with deformational plagiocephaly," *Pediatrics* **131**(1), e115 (2013).
6. B. L. Hutchison et al., "Serial developmental assessments in infants with deformational plagiocephaly," *J. Pediatr. Child Health* **48**(3), 274–278 (2012).
7. R. K. Kordestani et al., "Neurodevelopmental delays in children with deformational plagiocephaly," *J. Plast. Reconstr. Surg.* **117**(1), 207–218 (2006).
8. E. Courchesne et al., "Evidence of brain overgrowth in the first year of life in autism," *JAMA* **290**(3), 337–44 (2003).
9. L. M. Elder et al., "Head circumference as an early predictor of autism symptoms in younger siblings of children with autism spectrum disorder," *J. Autism Dev. Disorders* **38**(6), 1104–1111 (2008).
10. E. Fombonne et al., "Microcephaly and macrocephaly in autism," *J. Autism Dev. Disorders* **29**(2), 113–119 (1999).
11. S. M. Zahl et al., "Routine measurement of head circumference as a tool for detecting intracranial expansion in infants: what is the gain? A nationwide survey," *Pediatrics* **121**(3), e416–e420 (2008).
12. B. R. Collett et al., "Neurodevelopmental implications of 'deformational' plagiocephaly," *J. Dev. Behav. Pediatr.* **26**(5), 379 (2005).
13. M. Seruya et al., "Total cranial vault remodeling for isolated sagittal synostosis: part I. Postoperative cranial suture patency," *J. Plast. Reconstr. Surg.* **132**(4), 610e (2013).
14. D. R. Bronfin, "Misshapen heads in babies: position or pathology?" *Ochsner J.* **3**(4), 191–199 (2001).
15. G. H. Noritz et al., "Motor delays: early identification and evaluation," *Pediatrics* **131**(6), e2016–e2027 (2013).
16. L. Zwaigenbaum et al., "Early identification and interventions for autism spectrum disorder: executive summary," *Pediatrics* **136**(Suppl. 1), S1–S9 (2015).
17. "Top 6 benefits of early diagnosis in kids," http://www.kidsfirstraleigh.com/top-6-benefits-of-early-diagnosisscreening-tools/ (accessed 12 January 2018).
18. A. Ritter, "Positional plagiocephaly: prevention is key," *AAP Grand Rounds.* **32**(2), 24 (2014).
19. S. A. Gaetani, "A pediatric epidemic: deformational plagiocephaly/brachycephaly and congenital muscular torticollis," *Pediatrics* **36**(2), 10–18 (2009).
20. J. Carson et al., *Instruments of Science: An Historical Encyclopedia*, pp. 157–159, Taylor & Francis, New York (1998).
21. "Digital surface imaging® (DSi®) system," Cranial Technologies Inc., https://www.cranialtech.com/treatment/patient-experience (accessed 27 April 2021).
22. H. Schaaf et al., "Accuracy of photographic assessment compared with standard anthropometric measurements in nonsynostotic cranial deformities," *Cleft Palate-Craniofac. J.* **47**(5), 447–453 (2010).
23. E. N. Mortensen et al., "Interactive segmentation with intelligent scissors," *Graphical Models Image Process.* **60**(5), 349–384 (1998).

24. E. N. Mortensen et al., "Intelligent scissors for image composition," in *Proc. 22nd Annu. Conf. Comput. Graphics and Interactive Tech.*, ACM (1995).
25. E. W. Dijkstra, "A note on two problems in connexion with graphs," *Numer. Math.* **1**(1), 269–271 (1959).
26. W. Gonzalez et al., *Digital Image Processing Using MATLAB*, 3rd ed., Prentice Hall, New Jersey (2004).
27. J. Sato et al., "Affine reconstruction of curved surfaces from uncalibrated views of apparent contours," *IEEE Trans. Pattern Anal. Mach. Intell.* **21**(11), 1188–1198 (2000).

Reza Seifabadi is a co-founder and chief operating officer at PediaMetrix, Inc. He was a research fellow at the National Institutes of Health (NIH), where he developed state-of-the-art imaging and devices for prostate cancer diagnosis and treatment. He is a recipient of the SPIE Medical Imaging Best Poster Award in Ultrasound Tomography. He was trained as an entrepreneur in pediatric device innovation at Children's Hospital of Washington, DC, is an inventor of 7 US patents, and has extensively published in medical imaging, robotics, and image-guided interventions.

Fereshteh Aalamifar is the founder and CEO of PediaMetrix, Inc. She founded the company out of a personal experience as a mother. She holds a PhD in medical imaging and robotics from Johns Hopkins University (2016). She was a pre-doctoral fellow at NIH Clinical Center, when she developed the first co-robotic ultrasound tomography system for prostate cancer screening. She has served as a principal investigator (PI) for an SBIR Phase I Award, holds 3 US patents, and has published extensively in medical imaging, image-guided intervention, and robotics.

Seyed Hossein Hezaveh is a chief technology officer at PediaMetrix, Inc. He received his PhD from Princeton University in 2017 and has years of experience in algorithm development.

Can Kocabalkanli is a computer vision research engineer at PediaMetrix, Inc. He received a master's degree in robotics and a BSc degree in mechanical engineering from Johns Hopkins University in 2020 and 2019, respectively.

Kelly Wilburn is a practicing pediatrician at Dunwoody Pediatrics in Atlanta, Georgia. She is affiliated with multiple hospitals in the area, including Northside Hospital and Children's Healthcare of Atlanta. She received her medical degree from Baylor College of Medicine in 2001. She has been practicing general pediatrics since 2004. She is a fellow of the American Academy of Pediatrics.

Marius George Linguraru is co-founder and chief innovation officer at PediaMetrix Inc., a PI at Children's National Hospital, and a professor of radiology, pediatrics, and biomedical engineering at George Washington University. Trained at University of Oxford, Harvard University, and the NIH, he is an expert in quantitative imaging and AI for pediatric health.